

Received 6 November 2023, accepted 29 November 2023, date of publication 5 December 2023, date of current version 12 December 2023.

Digital Object Identifier 10.1109/ACCESS.2023.3339573

RESEARCH ARTICLE

A 2.4/5 GHz Dual-Band Low-Noise and Highly Linear Receiver With a New Power-Efficient Feedforward OPAMP for WiFi-6 Applications

SUKJU YUN¹, (Graduate Student Member, IEEE), JAEGEUN CHO^{1,2}, (Member, IEEE), SENGJUN JO¹, (Graduate Student Member, IEEE), IN-CHUL HWANG³, (Senior Member, IEEE), YOUNGJIN KIM⁴, (Senior Member, IEEE), SEONGHEON JEONG⁵, (Member, IEEE), JUNGEUN LEE⁵, (Member, IEEE), SANGHOON LEE⁵, (Member, IEEE), KEONTAE KIM⁵, (Member, IEEE), SEUNGYUP YOO⁵, (Member, IEEE), SANGWOO HAN⁵, (Member, IEEE), AND KUDUCK KWON¹, (Senior Member, IEEE)

¹Department of Electronics Engineering, Kangwon National University, Chuncheon 24341, South Korea

²Samsung Electronics Company Ltd., Hwaseong 18448, South Korea

³Department of Electrical Engineering, Kangwon National University, Chuncheon 24341, South Korea

⁴Department of Electronics Engineering, Korea Aerospace University, Goyang-si 10540, South Korea

⁵Supremicro Technologies Inc., Seoul 06742, South Korea

Corresponding author: Kuduck Kwon (kdkwon@kangwon.ac.kr)

This work was supported by Supremicro Technologies Inc.

ABSTRACT This paper presents a 2.4/5 GHz dual-band low-noise and highly linear receiver (RX) for IEEE 802.11a/b/g/n/ac/ax applications. The RX employs an RF front-end architecture composing a balun-low-noise transconductance amplifier, current-mode passive mixers, and transimpedance amplifiers (TIAs) to achieve compactness, low noise, and high linearity. A novel power-efficient feedforward operational amplifier architecture was also implemented in the TIA design to achieve the target RX error vector magnitude (EVM) of less than -35 dB with modulation and coding scheme 11 and 1024 quadrature amplitude modulation. Fabricated in a 22-nm SOI CMOS process, the RX achieved noise figures of 2.1/4.2 dB, in-band input-referred third-order intercept points of $-11.8/-7.5$ dBm, EVMs of $-46.4/-44.6$ dB for the 2.4/5 GHz bands, respectively. It drew a bias current of 21 mA from a nominal supply voltage of 0.8 V. The active die area was 0.65 mm².

INDEX TERMS Dual-band, error vector magnitude, feedforward operational amplifier, power-efficient, receiver, transimpedance amplifier, WiFi 6, WLAN, 802.11ax.

I. INTRODUCTION

The state-of-the-art technologies of the fourth industrial revolution, such as the Internet of Things, smart factories, virtual/augmented reality, remote offices, and cloud computing require smart devices with very high data throughput and low latency for wireless connection. Accordingly, WiFi standards are continuously developed from 802.11ac to 802.11ax and 802.11be to satisfy these demands and ensure high performance. A receiver (RX) error vector magnitude

The associate editor coordinating the review of this manuscript and approving it for publication was Tae Wook Kim¹.

(EVM) of -35 dB or less and channel bandwidth (CHBW) of 160 MHz must be ensured for modulation and coding scheme 11 (MCS11) 1024 quadrature amplitude modulation (QAM), to support 802.11ax [1], [2], [3], [4], [5]. An additional margin is required when considering the multipath fading environment. Therefore, the primary factors affecting the RX performance, such as circuit thermal noise, linearity, in-phase/quadrature (I/Q) gain and phase errors (i.e. image rejection ratio), local oscillator (LO) integrated phase noise, and in-band spurs must be significantly enhanced compared with those in 802.11ac [1], [2], [3], [4], [5]. Furthermore, to meet the target EVM floor requirement of MCS11, each

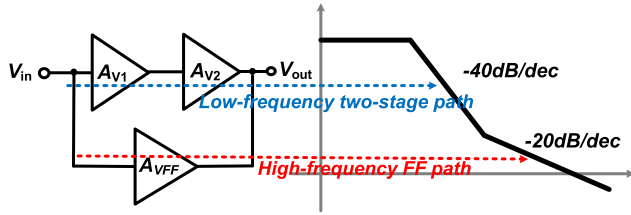


FIGURE 1. Block diagram and Bode plot of conventional two-stage FF OPAMP.

circuit block impairment contributing to the EVM should be 15 dB lower than the target EVM.

The current-driven passive mixer architecture has recently been used for high-performance receiving systems owing to its highly linear operation [1], [2], [3], [4], [5], [6], [7]. In this architecture, the overall performance (e.g., noise, linearity) of the RX signal path largely depends on the stage after the mixer, i.e., a transimpedance amplifier (TIA). Particularly, the TIA requires a high-performance operational amplifier (OPAMP) with a large voltage gain at the passband frequency range and large unity-gain frequency to support the CHBW of 160 MHz. In addition, the OPAMP should employ a power-efficient topology to reduce the RX power consumption.

This study proposes a 2.4/5 GHz dual-band low-noise and highly linear RX with a novel power-efficient feedforward (FF) OPAMP for IEEE 802.11a/b/g/n/ac/ax applications. The proposed WiFi RX employs an RF front-end architecture comprising a balun-low-noise transconductance amplifier (LNTA), current-mode passive mixers, and TIAs to achieve a small die size, low noise, and high linearity. This RF front-end architecture can achieve high linearity because the low input impedance of the TIA limits voltage swings at the mixer input and output. In addition, a new power-efficient FF OPAMP architecture is proposed and adopted in the TIA design to achieve low noise and high linearity for the RX chain. Section II describes the proposed power-efficient FF OPAMP architecture. Section III elaborates on the circuit implementation of the dual-band WiFi-6 RX. The experimental results are discussed in Section IV. The concluding remarks are presented in Section V.

II. NEW POWER-EFFICIENT FF OPAMP TOPOLOGY FOR THE HIGH-PERFORMANCE TIA

The FF OPAMP architecture reported in [8], [9], [10], and [11] is widely used for high-speed operation owing to its wide bandwidth and large voltage gain. The FF OPAMP phase can be compensated by a left-half-plane zero generated by the FF path without the Miller capacitance. Fig. 1 shows a simplified signal-path block diagram of the conventional FF OPAMP [8]. The FF and two-stage amplifier paths are observed on the -20 and -40 dB/dec lines at the Bode plot, respectively; consequently, the FF and the two-stage amplifier paths determine the characteristics of high and low frequencies, respectively. Fig. 2 shows the block diagrams of the conventional two-stage FF OPAMP topologies introduced in the previous

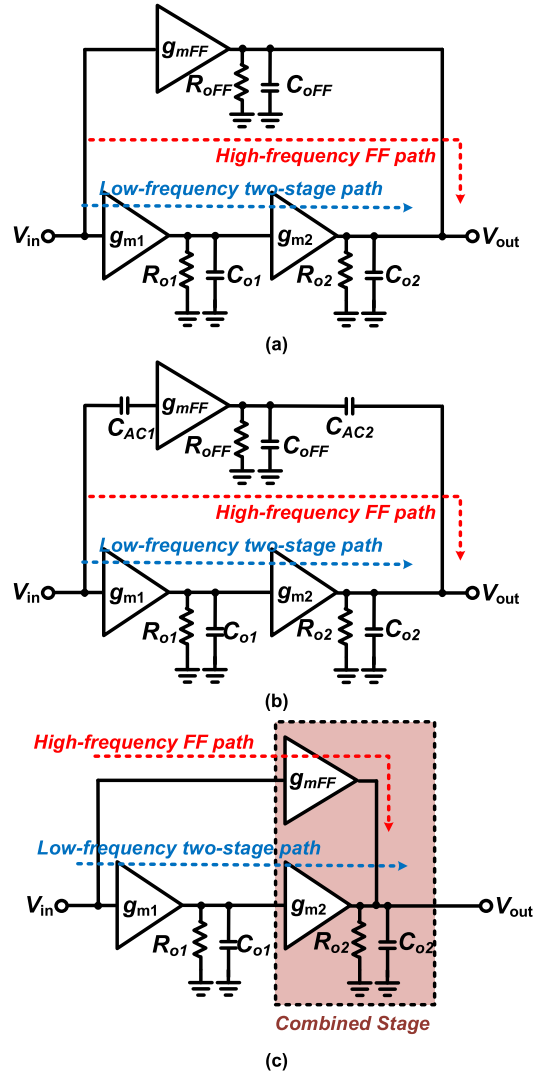


FIGURE 2. Block diagrams of conventional two-stage FF OPAMP topologies: (a) basic FF OPAMP topology (Version 1) [8] (b) modified FF OPAMP topology with ac coupling capacitors and current-reused g_{mFF} (Version 2) [9] (c) modified FF OPAMP topology with combined stage (Version 3) [11].

state-of-the-art. The basic two-stage FF OPAMP topology shown in Fig. 2(a) has the following transfer function:

$$H(s) \cong -\frac{(A_{V1}A_{V2} + A_{VFF})(1 + A_{VFF}s/(A_{V1}A_{V2} + A_{VFF})\omega_{p1})}{(1 + s/\omega_{p1})(1 + s/\omega_{p2})}, \quad (1)$$

where $A_{V1} = g_{m1}R_{o1}$, $A_{V2} = g_{m2}(R_{o2}||R_{oFF})$, and $A_{VFF} = g_{mFF}(R_{o2}||R_{oFF})$. $R_{o1,2,FF}$ and $C_{o1,2,FF}$ are the total resistance and capacitance at the output nodes of each stage, respectively. The dc gain, poles, and zero of the basic two-stage FF OPAMP topology (Version 1) are given by (2)–(5).

$$A_{dc, Ver1} = -(A_{V1}A_{V2} + A_{VFF}) \approx -g_{m1}R_{o1}g_{m2}(R_{o2}||R_{oFF}) \quad (2)$$

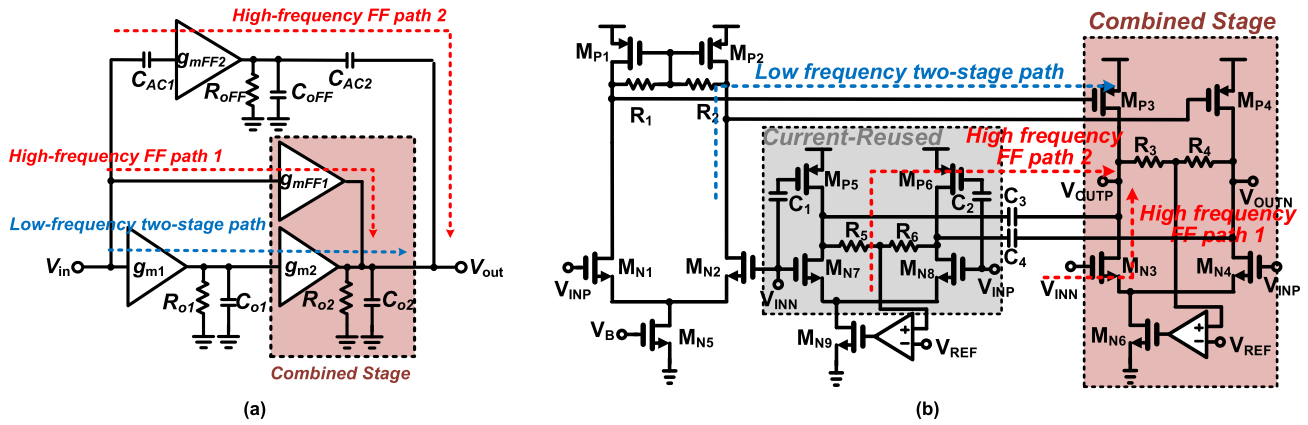


FIGURE 3. Proposed power-efficient FF OPAMP (Version 4): (a) block diagram (b) simplified schematic.

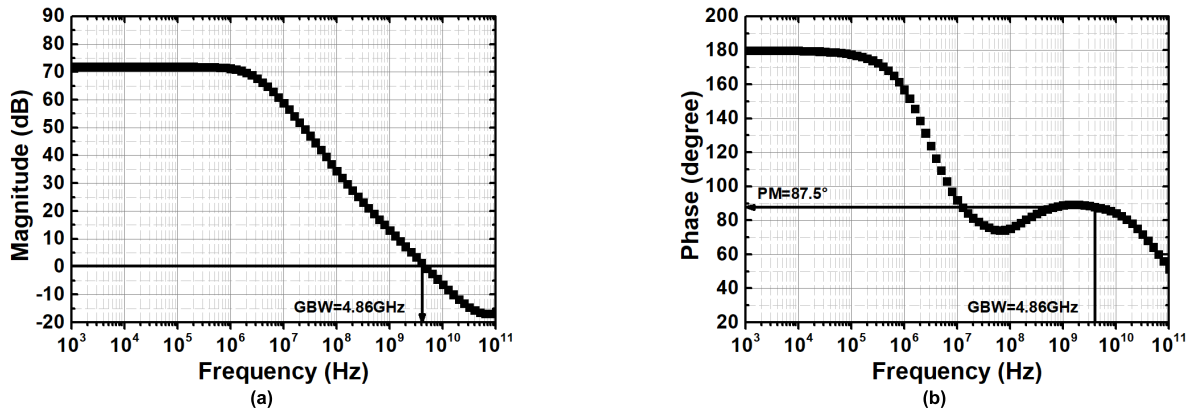


FIGURE 4. Simulated frequency response of the proposed FF OPAMP (a) magnitude (b) phase.

$$\omega_{p1,Ver1} = \frac{1}{R_{o1}C_{o1}} \quad (3)$$

$$\omega_{p2,Ver1} = \frac{1}{(R_{o2}||R_{oFF})(C_{o2} + C_{oFF})} \quad (4)$$

$$\omega_{z,Ver1} = \omega_{p1,Ver1} \left(1 + \frac{g_{m1}R_{o1}g_{m2}}{g_{mFF}} \right). \quad (5)$$

According to (2), the dc gain of the basic FF OPAMP is reduced owing to the parallel connection of R_{o2} and R_{oFF} . The dc gain is significantly reduced when the R_{oFF} value is comparable to or lower than R_{o2} . According to (5), a large g_{mFF} is necessary to move the $\omega_{z,Ver1}$ below unity-gain frequency (ω_t). Thus, realizing the phase compensation for sufficient phase margin requires a large current consumption. Accordingly, modified FF OPAMP topologies were introduced to address the two issues of the dc gain degradation and large current consumption of the FF stage [9], [10], [11]. The modified two-stage FF OPAMP topology employing ac coupling capacitors and current-reused g_{mFF} (Version 2), shown in Fig. 2(b), was introduced in [9]. The ac coupling capacitor, C_{AC2} , decouples the parallel connection of R_{o2} and R_{oFF} at dc. A current-reused CMOS (PMOS/NMOS) FF stage was also adopted to improve the power efficiency of the FF stage.

An ac coupling capacitor, C_{AC1} , was used to bias PMOS and NMOS transistors separately. The dc gain, poles, and zero of the modified two-stage FF OPAMP topology (Version 2) are given by (6)–(9).

$$A_{dc,Ver2} = -(A_{V1}A_{V2} + A_{VFF}) \approx -g_{m1}R_{o1}g_{m2}R_{o2} \quad (6)$$

$$\omega_{p1,Ver2} = \frac{1}{R_{o1}C_{o1}} \quad (7)$$

$$\omega_{p2,Ver2} \approx \frac{1}{(R_{o2}||R_{oFF})(C_{o2} + C_{oFF})} \quad (8)$$

$$\omega_{z,Ver2} = \omega_{p1,Ver2} \left(1 + \frac{g_{m1}R_{o1}g_{m2}}{g_{mFF}} \right). \quad (9)$$

The dc gain is improved, as shown in (6). The effective value of g_{mFF} of the current-reused CMOS FF stage is increased. That is, the current consumption required for the same g_{mFF} with the basic FF OPAMP topology (Version 1) is reduced. A modified FF OPAMP topology with a combined stage (Version 3), shown in Fig. 2(c), was also introduced to address the two issues [10], [11]. The modified topology of Version 3 combines a high-frequency FF path with the second stage of the low-frequency two-stage amplifier path. In this configuration, the load of the second stage of the

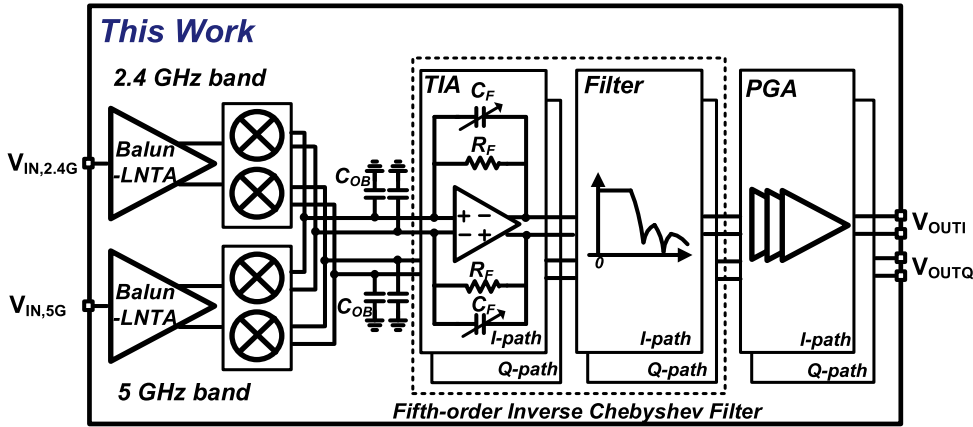


FIGURE 5. Block diagram of the proposed dual-band WiFi-6 receiver.

low-frequency two-stage amplifier acts as the G_m -stage of the high-frequency FF path, resulting in several advantages. First, the FF stage does not reduce the dc gain. Second, the combined stage improves power efficiency. In addition, the Version 3 topology effectively reduces the occurrence of internal poles and zeros caused by parasitic elements, limiting the bandwidth. The dc gain, poles, and zero of the modified two-stage FF OPAMP topology (Version 3) are given by (10)–(13).

$$A_{dc,Ver3} = -(A_{V1}A_{V2} + A_{VFF}) \approx -g_{m1}R_{o1}g_{m2}R_{o2} \quad (10)$$

$$\omega_{p1,Ver3} = \frac{1}{R_{o1}C_{o1}} \quad (11)$$

$$\omega_{p2,Ver3} \approx \frac{1}{R_{o2}C_{o2}} \quad (12)$$

$$\omega_{z,Ver3} = \omega_{p1,Ver3} \left(1 + \frac{g_{m1}R_{o1}g_{m2}}{g_{mFF}} \right). \quad (13)$$

This topology also improves dc gain, as shown in (10). According to (12), the total resistance increases, and the total capacitance decreases in the output node. Thus, $\omega_{p2,Ver3}$ is expected to be similar to $\omega_{p2,Ver1}$ and $\omega_{p2,Ver2}$.

A new FF OPAMP topology, shown in Fig. 3, is proposed. It comprises two high-frequency FF paths to further enhance power efficiency. The proposed FF OPAMP combines the key ideas of the previous modified FF OPAMP topologies. The additional high-frequency FF path with ac coupling capacitors C_{AC1} and C_{AC2} is employed in the modified FF OPAMP topology (Version 3) to further increase the effective g_m of the FF path, as shown in Fig. 3(a). C_{AC2} isolates the effect of the second FF path from the main low-frequency two-stage path at a low frequency; this prevents the gain reduction of the two-stage path caused by the second FF path. C_{AC2} gradually shortens the circuit with the increased operating frequency. The dc gain, poles, and zero of the proposed two-stage FF OPAMP topology (Version 4) are given by (14)–(17).

$$A_{dc,Ver4} = -(A_{V1}A_{V2} + A_{VFF}) \approx -g_{m1}R_{o1}g_{m2}R_{o2} \quad (14)$$

$$\omega_{p1,Ver4} = \frac{1}{R_{o1}C_{o1}} \quad (15)$$

$$\omega_{p2,Ver4} \approx \frac{1}{(R_{o2} \parallel R_{oFF})(C_{o2} + C_{oFF})} \quad (16)$$

$$\omega_{z,Ver4} = \omega_{p1,Ver4} \left(1 + \frac{g_{m1}R_{o1}g_{m2}}{(g_{mFF1} + g_{mFF2})} \right). \quad (17)$$

According to (17), the effective g_{mFF} increases to $g_{mFF1} + g_{mFF2}$. Fig. 3(b) shows a schematic of the proposed power-efficient FF OPAMP topology (Version 4). A current-reuse inverter-type amplifier was used to realize the G_m -stage of the second FF path (g_{mFF2}) to improve the current efficiency. $C_{3,4}$ functions as C_{AC2} to prevent dc gain reduction. The proposed FF OPAMP topology presents a larger effective g_m for the FF path than the modified FF OPAMP topologies (Versions 2 and 3) for the same current consumption, demonstrating the improvement in the phase margin. Generally, the power required to obtain a similar phase margin, dc gain, and high-frequency characteristics is reduced. The first and second stages used local and global common-mode feedback (CMFB) loops, respectively, to maintain the output common-mode voltage. The second FF stage also used a global CMFB loop. Fig. 4 shows the simulated frequency response of the proposed FF OPAMP. The simulated dc gain was 71.8 dB. The unity-gain frequency with a 0.1 pF loading effect of the following stage was 4.86 GHz, with an 87.5° phase margin. The voltage gains were 58.8, 51.9, 44.6, and 37 dB at 10, 20, 40, and 80 MHz, respectively. Therefore, the proposed FF OPAMP has sufficient voltage gain at the operating frequencies.

III. DUAL-BAND WIFI-6 RECEIVER

This section describes a circuit implementation of the 2.4/5 GHz dual-band low-noise and highly linear RX with a power-efficient FF OPAMP for IEEE 802.11a/b/g/n/ac/ax applications. Fig. 5 shows a simplified block diagram of the proposed RX. It comprises the 2.4/5 GHz balun-LNTAs, I/Q double-balanced current-mode passive mixers with 25% duty-cycle I/Q LO signals, I/Q TIAs, I/Q

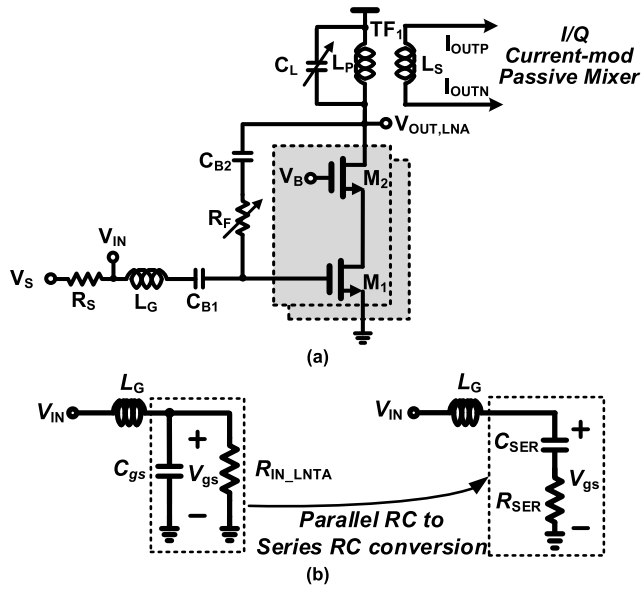


FIGURE 6. Schematic of the Q-booster resistive-feedback balun-LNTA.

fourth-order inverse Chebyshev active-RC low-pass filters (LPFs), and I/Q OPAMP-based programmable gain amplifiers (PGAs). C_{OB} suppresses the voltage swing of the out-of-band (OB) interferer on the RF and baseband sides of the mixer-switching transistors to improve the overall RX linearity [12], [13].

A. BALUN-LNTA

The 2.4/5 GHz balun-LNTAs employ a Q -boosted resistive feedback low-noise amplifier (RFLNA) topology with a series RLC input-matching network, as shown in Fig. 6 [14]. A 1:1 transformer, TF1, converts a single-ended voltage signal, $V_{OUT,LNA}$, into differential current signals, I_{OUTP} and I_{OUTN} . These current signals flowed into the double-balanced current-mode passive mixers with I/Q TIAs. The R_F provides the real part of the balun-LNTA input impedance. The balun-LNTA uses L_G to exploit the gain-boosting characteristics of an inductor-degenerated common-source LNA (L-CSLNA). The left subfigure of Fig. 6(b) shows a simplified diagram of the input-matching network of the balun-LNTA. The input impedance of the balun-LNTA R_{IN_LNTA} is expressed as

$$R_{IN_LNTA} = \frac{R_F + R_{oLNTA}}{(1 + g_{m1}R_{oLNTA})}, \quad (18)$$

where R_{oLNTA} is $Q_L\omega L_P \parallel g_{m2}r_{o2}r_{o1} \parallel R_{IN_MIXER}$ at the operating frequency. Q_L and R_{IN_MIXER} represent the quality factor of L_P and input impedance of the mixer, respectively. The right subfigure of Fig. 6(b) shows the equivalent input-matching network, converted through parallel RC -to-series RC conversion with a narrow frequency band of interest. Thus, the balun-LNTA performs input power matching with a series RLC network. The overall g_m of the balun-LNTA is effectively improved by $\sqrt{1 + Q_{SER}^2}$, where Q_{SER} is $\omega_o L_G / R_{SER}$ for an operational frequency of ω_o [14], [15].

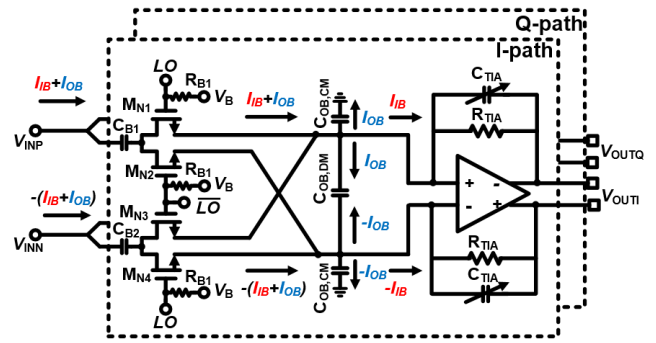


FIGURE 7. Schematic of the current-mode passive mixer with TIA.

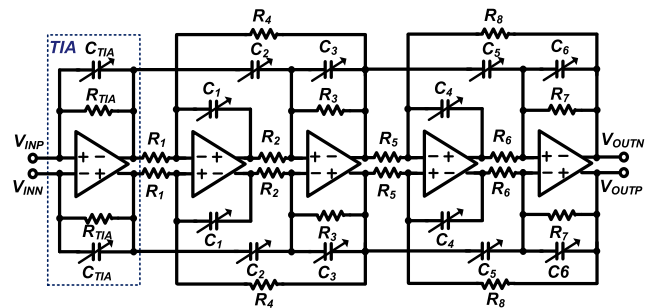


FIGURE 8. Schematic of the fifth-order Inverse Chebyshev LPF.

C_{SER} and R_{SER} are expressed as follows:

$$C_{SER} = C_{gs} \left(1 + \frac{1}{Q_{SER}^2} \right), \quad (19)$$

$$R_{SER} = \frac{R_F + R_{oLNTA}}{(1 + g_{m1}R_{oLNTA}) (1 + Q_{SER}^2)}. \quad (20)$$

When the L_G and C_{SER} values are set to resonate at the operating band, the input impedance of the balun-LNTA is obtained as R_{SER} , which must be equal to the source resistance, R_S . Therefore, the overall voltage gain of the RFLNA from V_S to $V_{OUT,LNA}$ is given as

$$A_{V,RFLNA} = -\frac{\sqrt{1 + Q_{SER}^2}}{2} \left(g_{m1} - \frac{1}{R_F} \right) (R_{oLNTA} \parallel R_F). \quad (21)$$

When $g_{m1}R_F \gg 1$, and $R_F \gg R_{oLNTA}$, $A_{V,RFLNA}$ can be approximated as

$$A_{V,RFLNA} \approx -\frac{\sqrt{1 + Q_{SER}^2}}{2} g_{m1}R_{oLNTA}. \quad (22)$$

The proposed RFLNA obtains a large voltage gain, similar to that of the L-CSLNA, while simultaneously removing the large on-chip spiral inductors at the source of M_1 . A resistor bank for R_F and G_m -cells comprising main and cascode transistors are digitally controlled for LNA gain control. In addition, C_L can be digitally tuned to adjust the center frequency of the LC load according to the operating band

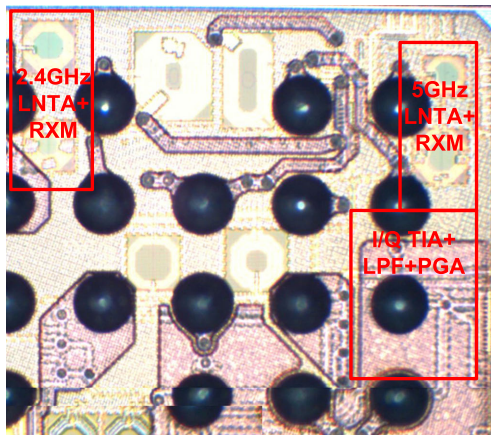


FIGURE 9. Chip microphotograph.

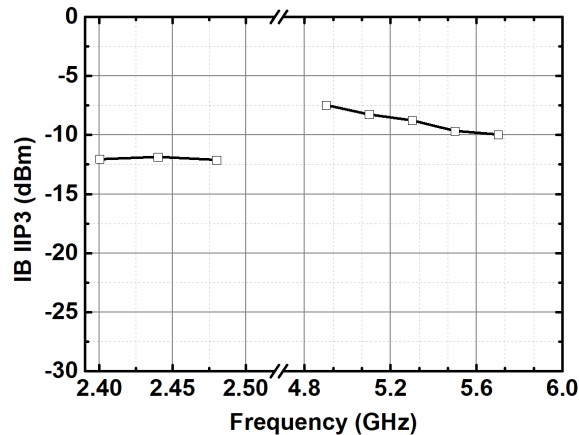


FIGURE 12. Measured IB IIP3.

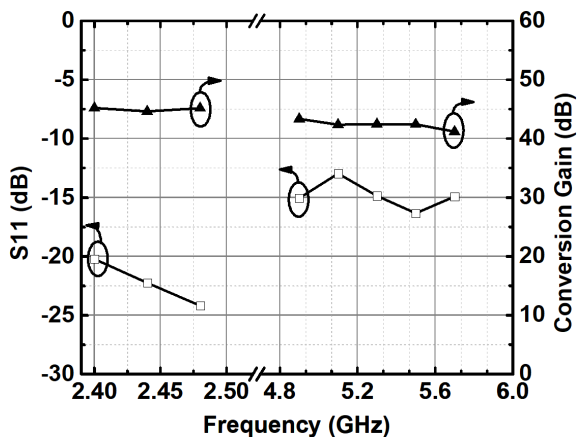


FIGURE 10. Measured S_{11} and conversion gain.

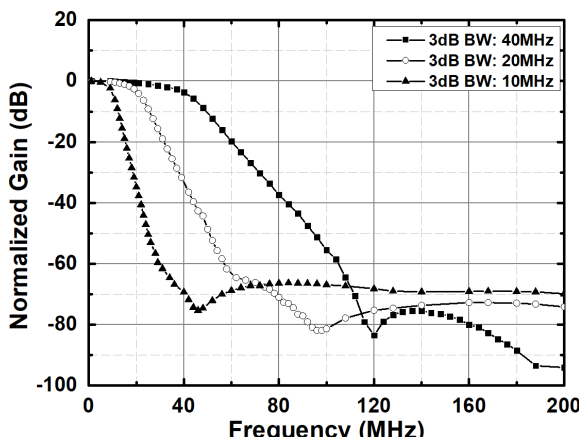


FIGURE 13. Measured IF frequency response versus filter bandwidth.

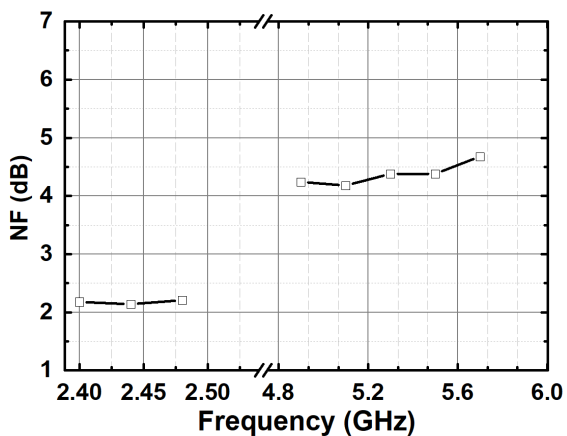


FIGURE 11. Measured NF.

B. CURRENT-MODE PASSIVE MIXER WITH TIA

The required linearity is achieved using double-balanced current-mode passive mixers with the TIA shown in Fig. 7 while maintaining the low impedances at the input and output of the mixer. The passive mixer also improves the

flicker noise performance owing to the absence of dc current. The ac-coupling capacitors (C_{B1} and C_{B2}) in front of the mixer-switching transistors perform high-pass filtering and reject the second-order intermodulation distortions generated by the preceding balun-LNTA. The I/Q mixers are driven by 25% duty-cycle quadrature LO signals provided by the divider and inverter-type LO buffers. The subsequent OPAMP-based TIA performs current-to-voltage conversion and eliminates the OB blockers and interfering signals. The OPAMP is the most important block because it determines the overall TIA performance, including the noise, linearity, and input impedance levels. Fig. 3 shows the proposed FF OPAMP with two high-frequency FF paths, adopted for the TIA to support an 80 MHz CHBW and achieve high linearity. The designed FF OPAMP can obtain a high voltage gain (even at high frequencies) and high unity-gain frequency for a given power consumption. As shown in Fig. 7, $C_{OB,DM}$ and $C_{OB,CM}$ are used to eliminate the differential-mode and common-mode OB interferers and blockers on the RF and baseband sides of the mixer-switching transistors to improve the overall RX linearity.

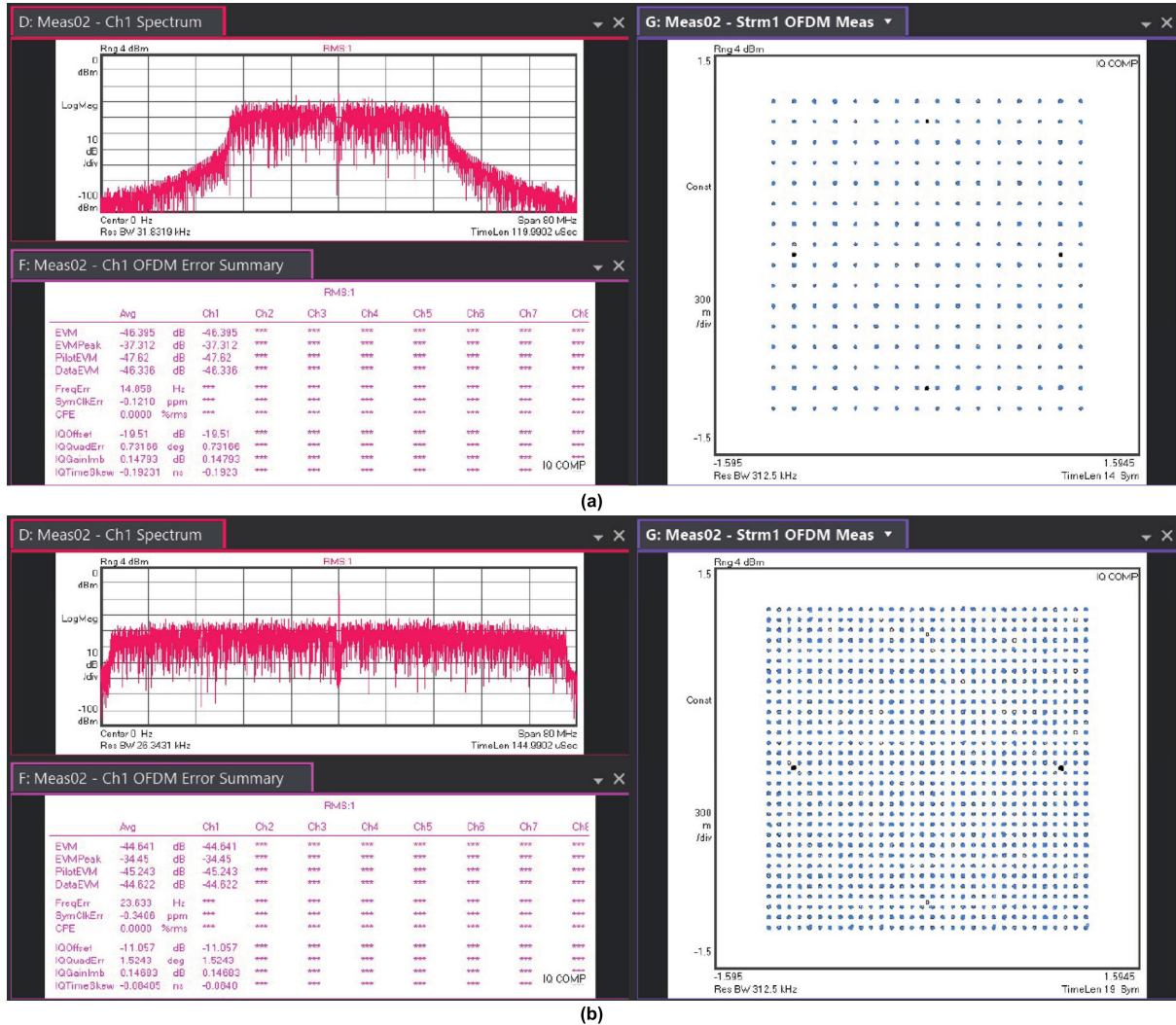


FIGURE 14. Measured EVMs and constellations: (a) 2.4 GHz band (MCS10 256QAM, CHBW = 40 MHz) (b) 5 GHz band (MCS11 1024QAM, CHBW = 80 MHz).

C. BASEBAND ANALOG CIRCUITS

As shown in Fig. 8, an active-RC LPF with the preceding TIA implements a fifth-order inverse Chebyshev LPF. It can provide an adjacent channel rejection ratio (ACRR) of more than 35 dB. The 3 dB filter bandwidth can be tuned to 10, 20, and 40 MHz based on the WiFi channel bandwidth. A three-stage OPAMP-based PGA is used to provide a 42 dB maximum voltage gain with a 60 dB dynamic range and 1 dB gain step.

IV. EXPERIMENTAL RESULTS

The dual-band WiFi-6 RX was fabricated using 22-nm silicon on insulator complementary metal-oxide semiconductor (SOI CMOS) technology. Fig. 9 shows a microphotograph of the chip. The RX has an active die area of 0.65 mm² including 2.4/5 GHz LNTAs/RXMs and I/Q TIAs/LPFs/PGAs. The 2.4/5 GHz RX, excluding the LO circuits, drew a current of 21/20.5 mA from a nominal supply voltage of 0.8 V. The current consumptions of the 2.4/5 GHz balun-LNTA, I/Q

TIAs, I/Q active-RC LPFs, and three-stage PGAs were 4/3.5, 3, 8, and 6 mA, respectively. A grounded 50-Ω coplanar waveguide was applied on an assembled printed circuit board to perform the measurements. The differential LO signals at 2f_{LO} were supplied from the off-chip through a commercial balun.

Fig. 10 shows the measured S₁₁ and conversion gain of the RX when the baseband analog circuits have a 0 dB gain code. The implemented RX achieved a measured S₁₁ of less than -10 dB and a conversion gain of 42–45 dB. Fig. 11 showed the measured double side-band (DSB) NFs versus the operating RF frequencies. The RX achieves minimum NFs of 2.1/4.2 dB at the 2.4/5 GHz bands, respectively. The RX in-band (IB) input-referred third-order intercept points (IIP3) were also characterized by adjacent and alternate channels. The two-tone test conditions of the IB IIP3 for 2.4 GHz band and 20 MHz CHBW were f₁ = f_{LO} + 20 MHz, f₂ = f_{LO} + 41 MHz, p_{f1} = -60 dBm, and p_{f2} = -44 dBm. The two-tone test conditions of the IB IIP3 for the 5 GHz

TABLE 1. Measured performance summaries and comparisons.

Reference		[1] ISSCC 2020	[2] ISSCC 2018	[3] RFIC 2018	[4] RFIC 2023	[5] JSSC 2017	This work
Supported WiFi Standard		802.11 a/b/g/n/ac/ax	802.11 a/b/g/n/ac/ax	802.11 a/b/g/n/ac/ax	802.11 a/b/g/n/ac/ax/be	802.11 a/b/g/n/ac	802.11 a/b/g/n/ac/ax
Technology		CMOS 55nm	CMOS 28nm	CMOS 28nm	CMOS 55nm	CMOS 40nm	SOI CMOS 22nm
RX NF (dB)	2.4G	4.2	2.9	3.7	3.5	2.9	2.1
	5G	4.8	3.2	3.8	4.5	4.5	4.2
IB IIP3 (dBm)	2.4G	NA [†]	NA	NA	NA	NA	-11.8
	5G	NA	NA	NA	NA	NA	-7.5
P _{ac} [mW]	2.4G	322	354 (4SS*+1LO)	NA	254 (1SS)	179 (2SS)	16.8 (1SS RX only)
	5G	420 (4SS+1LO)	447 (4SS+2LO)	NA	359 (1SS)	243 (2SS)	16.4 (1SS RX only)
Area (mm ²)		22.9 (4SS)	12 (4SS)	11.7 (2SS+BT+FM)	3.74 (1SS)	8.6 (2SS+BT)	0.65 (1SS RX only)

†NA = not available *spatial stream

band and 80 MHz CHBW were $f_1 = f_{LO} + 80$ MHz, $f_2 = f_{LO} + 161$ MHz, $p_{f1} = -57$ dBm, and $p_{f2} = -41$ dBm. The two-tone test conditions are derived from the frequencies and powers of the adjacent and alternate adjacent channels. The obtained maximum IB IIP3s were $-11.8/-7.5$ dBm for the 2.4/5 GHz bands, respectively, as shown in Fig. 12. Fig. 13 shows the measured baseband frequency responses for different filter bandwidth modes. The proposed RX can support three bandwidth modes of 10/20/40 MHz. Fig. 14 shows the measured RX EVMs, received spectrums, and constellations for the 2.4/5 GHz bands. MCS10 256QAM/40 MHz CHBW and MCS11 1024QAM/80 MHz CHBW signals were used for the 2.4/5 GHz bands, respectively. The measured RF input power was -50 dBm for both bands. The obtained minimum RX EVMs were $-46.4/-44.6$ dB for the 2.4/5 GHz bands, respectively. The measured RX EVMs for the 2.4/5 GHz bands were much less than the target EVM of -35 dB. Table 1 presents a comparison of the performance of the proposed RX with those of other reported WiFi RXs. The implemented RX obtained similar or better noise performance compared to other WiFi RXs

V. CONCLUSION

A 2.4/5 GHz dual-band low-noise and highly linear RX for IEEE 802.11a/b/g/n/ac/ax applications was designed and implemented in a 22-nm SOI CMOS process. A new power-efficient FF OPAMP architecture was proposed to achieve a broadband, low-noise, and highly linear TIA. The proposed RX obtained a maximum conversion gain of 85 dB with a dynamic range of 120 dB, a gain step of 1 dB, and an ACRR of more than 35 dB. It also achieved NFs of 2.1/4.2 dB and IB IIP3s of $-11.8/-7.5$ dBm for the 2.4/5 GHz bands, respectively.

ACKNOWLEDGMENT

The authors would like to thank all the members for their support and fruitful discussions.

REFERENCES

- [1] E. Ru, W. Li, Z. Deng, E. Rostami, P. Wu, K. Chang, Y. Chuang, C. Lai, Y. Chen, T. Peng, T. Tsai, H. Liu, C. Chiu, B. Huang, Y. Wang, J. Zhan, and O. Shanna, "A 4×4 dual-band dual-concurrent WiFi 802.11ax transceiver with integrated LNA, PA and T/R switch achieving $+20$ dBm 1024-QAM MCS11 pout and -43 dB EVM floor in 55 nm CMOS," in *IEEE Int. Solid-State Circuits Conf. (ISSCC) Dig. Tech. Papers*, Feb. 2020, pp. 178–179.
- [2] S. Kawai et al., "An 802.11ax 4×4 spectrum-efficient WLAN AP transceiver SoC supporting 1024 QAM with frequency-dependent IQ calibration and integrated interference analyzer," in *IEEE Int. Solid-State Circuits Conf. (ISSCC) Dig. Tech. Papers*, Feb. 2018, pp. 442–444.
- [3] C. Wu et al., "A 28 nm CMOS wireless connectivity combo IC with a reconfigurable 2×2 MIMO WiFi supporting 80+80 MHz 256-QAM, and BT 5.0," in *Proc. IEEE RFIC*, Jun. 2018, pp. 300–303.
- [4] T. Chen, M. Liu, P. Wu, W. Hong, T. Liang, W. Chao, P. Chang, Y. Chou, C. Chen, S. Liu, C. Huang, H. Ting, M. Hsu, Y. Wang, C. Hung, Y. Hsueh, E. Lu, and Y. Chung, "A Wi-Fi tri-band switchable transceiver with 57.9 fs-RMS-jitter frequency synthesizer, achieving -42.6 dB EVM floor for EHT320 4096-QAM MCS13 signal," in *Proc. IEEE RFIC*, Jun. 2023, pp. 181–184.
- [5] S. Yan, L. Ye, R. Kulkarni, E. Myers, H. Shih, H. Wu, S. Saberi, D. Kadia, D. Ozis, L. Zhou, E. Middleton, and J. Tham, "An 802.11a/b/g/n/ac WLAN transceiver for 2×2 MIMO and simultaneous dual-band operation with $+29$ dBm P_{sat} integrated power amplifiers," *IEEE J. Solid-State Circuits*, vol. 52, no. 7, pp. 1798–1813, Jul. 2017.
- [6] J. Han and K. Kwon, "I/Q balance-enhanced wideband receiver front-end for 2G/3G/4G/5G NR cellular applications," *IEEE Trans. Circuits Syst. I, Reg. Papers*, vol. 67, no. 6, pp. 1881–1891, Jun. 2020.
- [7] J. Han and K. Kwon, "RF receiver front-end employing IIP2-enhanced 25% duty-cycle quadrature passive mixer for advanced cellular applications," *IEEE Access*, vol. 8, pp. 8166–8177, 2020.
- [8] J. Harrison and N. Weste, "A 500 MHz CMOS anti-alias filter using feed-forward op-amps with local common-mode feedback," in *IEEE Int. Solid-State Circuits Conf. (ISSCC) Dig. Tech. Papers*, Feb. 2003, pp. 132–133.
- [9] H. Jung, D. R. Utomo, S.-K. Han, J. Kim, and S.-G. Lee, "An 80 MHz bandwidth and 26.8 dBm OOB IIP3 transimpedance amplifier with improved nested feedforward compensation and multi-order filtering," *IEEE Trans. Circuits Syst. I, Reg. Papers*, vol. 67, no. 10, pp. 3410–3421, Oct. 2020.
- [10] K. Kwon, "A 40 M-1000 MHz 77.2-dB spurious free dynamic range CMOS RF variable gain amplifier for digital TV tuner ICs," *Int. J. Circuit Theory Appl.*, vol. 43, no. 7, pp. 875–886, Jul. 2015.
- [11] D. Shin, K. Lee, and K. Kwon, "A blocker-tolerant receiver front end employing dual-band N-path balun-LNA for 5G new radio cellular applications," *IEEE Trans. Microw. Theory Techn.*, vol. 70, no. 3, pp. 1715–1724, Mar. 2022.
- [12] K. Kwon and J. Han, "A 2G/3G/4G SAW-less receiver front-end adopting switchable front-end architecture," *IEEE Trans. Microw. Theory Techn.*, vol. 62, no. 8, pp. 1716–1723, Aug. 2014.

- [13] J. Deguchi, D. Miyashita, Y. Ogasawara, G. Takemura, M. Iwanaga, K. Sami, R. Ito, J. Wadatsumi, Y. Tsuda, S. Oda, S. Kawaguchi, N. Itoh, and M. Hamada, "A fully integrated 2×1 dual-band direct-conversion mobile Wimax transceiver with dual-mode fractional divider and noise-shaping transimpedance amplifier in 65 nm CMOS," *IEEE J. Solid-State Circuits*, vol. 45, no. 12, pp. 2774–2784, Dec. 2010.
- [14] S. Joo, T.-Y. Choi, and B. Jung, "A 2.4-GHz resistive feedback LNA in 0.13- μm CMOS," *IEEE J. Solid-State Circuits*, vol. 44, no. 11, pp. 3019–3029, Nov. 2009.
- [15] B. Razavi, *RF Microelectronics*. Upper Saddle River, NJ: Prentice-Hall, 1998.
- [16] R. Schaumann and M. Valkenburg, *Design of Analog Filters*. Oxford, U.K.: Oxford Univ. Press, 2001.



on designing low-noise broadband WiFi-6/7 receivers and blocker-tolerant receiver for 5G NR cellular applications.

SUKJU YUN (Graduate Student Member, IEEE) received the B.S. and M.S. degrees from the Department of Electronics Engineering, Kangwon National University, Chuncheon, South Korea, in 2020 and 2022, respectively, where he is currently pursuing the Ph.D. degree with the Department of Electronics Engineering.

His research interests include CMOS mmWave/RF/analog integrated circuits and RF system design for wireless communications. He focuses

JAEGEUN CHO (Member, IEEE) received the integrated B.S. and M.S. degrees from the Department of Electronics Engineering, Kangwon National University, Chuncheon, South Korea, in 2023.

Since 2023, he has been with Samsung Electronics Company Ltd., Hwaseong, Gyeonggi-do, South Korea. His research interests include CMOS mmWave/RF/analog integrated circuits and RF system design for wireless communications.

SENGJUN JO (Graduate Student Member, IEEE) is currently pursuing the integrated B.S. and M.S. degrees with the Department of Electronics Engineering, Kangwon National University, Chuncheon, South Korea.

His research interests include CMOS mmWave/RF/analog integrated circuits and RF system design for wireless communications. He focuses on designing a blocker-tolerant receiver for 5G NR cellular applications and WiFi-6/7 receivers.

IN-CHUL HWANG (Senior Member, IEEE) received the B.S., M.S., and Ph.D. degrees from Korea University, Seoul, South Korea, in 1993, 1995, and 2000, respectively.

He was a Postdoctoral Associate with the Coordinated Science Laboratory, University of Illinois at Urbana-Champaign, Urbana, IL, USA, from 2000 to 2001. In 2001, he joined Samsung Electronics, System LSI Division, Giheung-gu, South Korea. Since 2007, he has been with the

Department of Electrical and Electronics Engineering, Kangwon National University, Chuncheon, South Korea, where he is currently a Professor. He was a Visiting Scholar with the Georgia Institute of Technology, Atlanta, GA, USA, in 2012. His current research interests include digital PLL for RFIC and digital LDO for dynamic-voltage and frequency scaling applications.



YOUNGJIN KIM (Senior Member, IEEE) received the B.S. degree in electrical engineering from Kyungpook National University, in 1995, and the M.S. and Ph.D. degrees in electrical engineering from the Korea Advanced Institute of Science and Technology (KAIST), in 1997 and 2002, respectively. His Ph.D. dissertation focused on the transceiver architecture of image rejection and spurious rejection. In 2002, he joined Samsung Electronics Company Ltd., South Korea, as a Senior Engineer. Since then, he has participated in the design of CDMA and GSM/GPRS wireless mobile applications. Furthermore, he has designed a LNA and down-conversion mixer for multi-mode CDMA and GSM/GPRS. In 2006, he joined the School of Electronics and Information Engineering, Korea Aerospace University, Goyang-si, South Korea.



SEONGHEON JEONG (Member, IEEE) received the B.S. and M.S. degrees in electrical engineering from Soongsil University, Seoul, in 2005 and 2007, respectively. From 2007 to 2019, he was a Senior Engineer with Future Communications IC (FCI) Inc., Sungnam-si, South Korea, where he has been involved with the development of TDMB SoC, ISDB-T, and Wi-Fi SoC product using CMOS RF process. From 2019 to 2021, he was a Senior Engineer with Dialog Semiconductor, Pangyo, South Korea, where he has been involved with the development of Bluetooth SoC and Wi-Fi SoC product using CMOS RF. In 2021, he joined the RF/analog Team, Supremicro Technologies Inc., Seoul, South Korea, where he is currently a Senior Engineer and involved in the development of Wi-Fi SoC product.



JUNGEUN LEE (Member, IEEE) received the B.S. and M.S. degrees in semiconductor science from Dongguk University, Seoul, South Korea, in 1998 and 2000, respectively. From 2000 to 2010, he was a member of Technical Staff with the Samsung Advanced Institute of Technology (SAIT), Yongin-si, South Korea, where he was the Technical Leader of the Mixed Signal Group. From 2010 to 2017, he was the Co-Founder and the CTO of RF Analog Mixed IC Solutions (RAMICS) Inc., Sungnam-si, South Korea, where he designed CMOS integrated circuits involving synthesizer, data converters, and receiver architectures for broadcast systems and developed the CMOS hybrid (analog and digital) TV tuner. From 2017 to 2021, he was the Director of the Analog Team, Future Communications IC (FCI) Inc., Sungnam-si, South Korea, where he developed the data converters and synthesizer for bluetooth SoC and Wi-Fi SoC products. In 2021, he co-founded Supremicro Technologies Inc., Seoul, where he is currently leading the development Wi-Fi SoC product.



SANGHOON LEE (Member, IEEE) received the B.S. and M.S. degrees in electrical engineering from Incheon University, Incheon, in 1999 and 2001, respectively. From 2001 to 2019, he was a Principal Research Engineer with Future Communications IC (FCI) Inc., Sungnam-si, South Korea, where he has been involved with the development of CDMA RF, SDMB/TDDB RF products using SiGe BICMOS process, LTE transceiver, and Wi-Fi SoC product using CMOS RF process. From 2019 to 2021, he was a Principal Research Engineer with Dialog Semiconductor, Pangyo, South Korea, where he has been involved with the development of bluetooth SoC and Wi-Fi SoC product using CMOS RF process. In 2021, he joined the RF/Analog Team, Supremicro Technologies Inc., Seoul, South Korea, where he is also involved in the development of Wi-Fi SoC product.



KEONTAE KIM (Member, IEEE) received the B.S. and M.S. degrees in computer engineering from Pusan National University, Busan, in 2004 and 2006, respectively. From 2006 to 2010, he was with I&C Technology Company Ltd., Seoul, where he was an Assistant Research Engineer and worked on modem team. From 2015 to 2017, he was a Research Engineer with RAMIC Inc., Sungnam-si, South Korea, where he has been involved with the development digital block of TV tuner. From 2017 to 2019, he was a Research Engineer with Future Communications IC (FCI) Inc., Sungnam-si, where he has been involved with digital supported ADC and DAC. From 2019 to 2021, he was a Senior Research Engineer with Dialog Semiconductor Wi-Fi Operations, Pangyo, South Korea, where he has been involved with development of digital supported ADC and DAC and full chip verification. In 2021, he joined the RF/Analog Team, Supremicro Technologies Inc., Seoul, South Korea, where he is currently a Principle Research Engineer and involved in the development of Wi-Fi SoC product.



SANGWOO HAN (Member, IEEE) received the B.S. degree from CMU, the M.S. degree from the University of Pennsylvania, and the Ph.D. degree in electronics engineering from the Georgia Institute of Technology. In 1997, he co-founded RF Solutions Inc., Atlanta, GA, USA, which became the Anadigics Wireless LAN Center of Excellence, in 2003. From 2003 to 2008, he was in charge of product design, development, production, and marketing with Future Communications IC (FCI) Inc., which was acquired by Silicon Motion, in April 2007. From 2008 to 2019, he was a SVP and the General Manager of the Silicon Motion Mobile Communications Business Unit which was acquired by Dialog Semiconductor, in June 2019. From 2019 to 2020, he was a VP of the Dialog Semiconductor IoT Wi-Fi Business Unit. Since 2021, he has been a VP of Supremicro Technologies Inc.



SEUNGYUP YOO (Member, IEEE) received the B.S. and M.S. degrees in electrical engineering from Hanyang University, Seoul, in 1992 and 1994, respectively, and the Ph.D. degree in electrical and computer engineering from the Georgia Institute of Technology, Atlanta, GA, USA, in 2000. From 2000 to 2003, he was with RF Solutions Inc., Atlanta, where he was a Staff Engineer and worked on GaAs MESFET and SiGe BiCMOS RFIC designs for wireless data applications. From 2003 to 2019, he was the Senior Executive Director of Future Communications IC (FCI) Inc., Sungnam-si, South Korea, where he has been involved with the development of SiGe BiCMOS RF wireless transceivers, mobile TV SiP module and SoC, CDMA/LTE products, and Wi-Fi SoC product using CMOS RF process and also led operation teams. From 2019 to 2021, he was the Senior Director of Dialog Semiconductor Wi-Fi Operations, Pangyo, South Korea, where he led operation teams and has been involved in project management. In 2021, he joined the RF/Analog Team, Supremicro Technologies Inc., Seoul, South Korea, where he is currently the Project Manager and involved in the development of Wi-Fi SoC product.



KUDUCK KWON (Senior Member, IEEE) received the B.S. and Ph.D. degrees in electrical engineering and computer science from the Korea Advanced Institute of Science and Technology (KAIST), Daejeon, South Korea, in 2004 and 2009, respectively. His Ph.D. research concerned digital TV tuners and dedicated short-range communication (DSRC) systems. From 2009 to 2010, he was a Postdoctoral Researcher with KAIST, where he studied a surface acoustic wave (SAW)-less receiver architectures and developed 5.8 GHz RF transceivers for DSRC applications. From 2010 to 2014, he was a Senior Engineer with Samsung Electronics Company Ltd., Suwon, South Korea, where he has been involved with studies of the SAW-less software-defined receivers and development of CMOS transceivers for 2G/3G/4G cellular applications and receivers for universal silicon tuners. In 2014, he joined the Department of Electronics Engineering, Kangwon National University, Chuncheon, South Korea, where he is currently a Professor. His research interests include CMOS mmWave/RF/analog integrated circuits and RF system design for wireless communications.

...